CALCULATION OF THREE-DIMENSIONAL COMPRESSIBLE LAMINAR AND TURBULENT BOUNDARY LAYERS

AN IMPLICIT FINITE-DIFFERENCE PROCEDURE FOR SOLVING THE THREE-DIMENSIONAL COMPRESSIBLE LAMINAR, TRANSITIONAL, AND TURBULENT BOUNDARY-LAYER EQUATIONS

By Julius E. Harris
NASA Langley Research Center

SUMMARY

An implicit finite-difference procedure is presented for solving the compressible three-dimensional boundary-layer equations. The method is second-order accurate, unconditionally stable (conditional stability for reverse cross flow), and efficient from the viewpoint of computer storage and processing time (60000_8 storage and 0.002 second per nodal point on the CDC 6600 computer). The Reynolds stress terms are modeled by (1) a single-layer mixing length model and (2) a two-layer eddy viscosity model. These models, although simple in concept, accurately predicted the equilibrium turbulent flow for the conditions considered. Numerical results are compared with experimental wall and profile data for a cone at an angle of attack larger than the cone semiapex angle. These comparisons clearly indicate that the numerical procedure and turbulence models accurately predict the experimental data with as few as 21 nodal points in the plane normal to the wall boundary. Research continues in the areas of convergence accelerator techniques (reduction of computer processing time), turbulence modeling, and extension of the computer code to general configurations (general geometry package development).

INTRODUCTION

A current design and analysis requirement of the aerospace industry is development of accurate and efficient numerical techniques and corresponding user-oriented computer codes for solving the compressible three-dimensional laminar, transitional, and turbulent boundary-layer equations for flows over general configurations. These codes would substantially reduce the cost and time currently required for the development of advanced aircraft through the substitution of numerical simulation for time-consuming and expensive experimental simulation and testing. The research focused on three-dimensional boundary-layer flows can be attributed to (1) experience gained over

the past decade in developing user-oriented codes for two-dimensional and axisymmetric flows, including the development of numerical procedures and simple but accurate mean-field turbulence models and (2) the increased availability of large-storage high-speed digital computer systems.

Experience gained in two-dimensional and axisymmetric boundary-layer flows indicates that computer codes for three-dimensional turbulent flows, if they are to be accepted as design/analysis tools by the aerospace industry, will require efficient and accurate numerical methods with suitable turbulence models for the Reynolds stresses. Numerical experimentation and detailed experimental turbulent boundary-layer research has resulted in the development and verification of mean-field turbulence models (eddy viscosity/mixing length) for two-dimensional boundary-layer flows which are sufficiently accurate for application to a broad range of flow and boundary conditions. (See refs. 1 to 4.) The numerical techniques developed for this class of flow can be directly applied, with minor modifications, to three-dimensional flows; however, zones of dependence and independence must be carefully treated for three-dimensional flows (see refs. 5 and 6). Although the extension of two-dimensional mean-field turbulence models to three-dimensional flows appears to be straightforward, numerical experimentation in which numerical results are compared with accurate three-dimensional profile and wall data is required before any evidence can be produced to prove or disprove this assumption (refs. 7 to 9).

If one assumes that accurate and efficient numerical procedures together with sufficiently realistic turbulence models can be developed on the basis of experience with two-dimensional flows, a number of problem areas still remain to be solved for general three-dimensional boundary-layer flows; these include: (1) selection and development of an optimum boundary-layer coordinate system; (2) development of general transformations which will remove numerical problems associated with the generation of initial data planes, reduce the growth of the boundary layer in the computational region, and reduce the sensitivity of the numerical procedure to mesh-point distributions in the two spatial surface coordinates; and (3) availability and/or use of accurate three-dimensional inviscid flow-field solutions which are required for edge boundary condition specification. (See ref. 10.) Problems associated with (1) and (3) make it manditory that the boundary-layer codes be coupled with the three-dimensional inviscid flow-field codes to avoid excessive and time-consuming data manipulation as well as to provide the possibility of accounting for displacement surface effects on numerical results. For general aerospace configurations the problem associated with obtaining accurate three-dimensional inviscid flow-field data may well be the most difficult. However, substantial progress has been made in this particular area of research. Progress has also been made in the area of three-dimensional boundary-layer flows over the past few years (refs. 11 to 15). A crit-

ical review of computational techniques for boundary-layer flows (two- and three-dimensional) is presented in reference 16.

In this paper a technique under development at the NASA Langley Research Center for solving the compressible three-dimensional laminar, transitional, and turbulent boundary-layer equations is presented. The advantages and disadvantages of the implicit finite-difference procedure and Crocco transformation are discussed. The Reynolds stress terms are modeled by two mean-field (scalar invariant) models. Numerical results are presented and compared with experimental data to determine the validity of the simple turbulence models and the accuracy of the numerical procedure.

SYMBOLS

A	damping term in turbulence model (eq. (12))
a_1,a_2	coefficients in boundary condition on shear equation (see eq. (25b))
C	coefficient of geometric progression for mesh-point distribution, $\Delta\zeta_{k+1}/\Delta\zeta_k$
$C_{f,e}$	skin-friction coefficient
c_p	specific heat at constant pressure
D	Van Driest damping factor (eq. (11))
ds	incremental arc length
$\bar{e}$	$= \frac{\mu}{T}\left(1 + \frac{\epsilon}{\mu}\Gamma\right)$
F	$= u/u_e$
G	$= v/v_e$
H	$= w/u_e$
h_1,h_2,h_3	metric coefficients (eq. (5))

$k_1, k_2, \ldots, k_6$ coefficients in turbulence models (eqs. (9) to (17))

$\bar{k}_{eff}$ effective thermal conductivity (eq. (8))

$\bar{L}$ reference length

ℓ_1, ℓ_2 mixing lengths (eqs. (10) and (17))

M_∞ free-stream Mach number

N number of mesh points in the plane normal to the wall boundary

N_{Pr} Prandtl number

$N_{Pr,t}$ static turbulent Prandtl number

p pressure

$R_{\infty,L}$ Reynolds number based on reference length

T temperature

$\bar{U}_\infty$ free-stream velocity

$U_{e,t}$ total velocity at edge of boundary layer

u, v, w velocity component in the ξ-, η-, and ζ-direction, respectively

x_1, x_2, x_3 physical coordinates

$Y_1, Y_2, \ldots, Y_6$ coefficients for derivative relations (eqs. (33) to (38))

$\bar{\alpha}$ angle of attack

$\alpha_1, \alpha_2, \ldots, \alpha_5$ coefficients in standard equation (eq. (24))

$\beta_1,\beta_2,\beta_3,\beta_4$	coefficients in equation (40)
γ	ratio of specific heats
$\tilde{\gamma}$	normal intermittency function (eq. (13))
Γ	streamwise intermittency function
$\Delta\xi,\Delta\eta,\Delta\zeta$	incremental mesh-point spacing in the ξ,η,ζ coordinates
$\bar{\delta}^*$	incompressible displacement thickness (eq. (19))
ϵ	eddy viscosity
ζ	transformed normal coordinate
η	transformed cross-flow coordinate
θ	$= T/T_e$
κ_1,κ_2	geodesic curvatures (eq. (6))
μ	molecular viscosity
$\bar{\mu}_{eff}$	effective viscosity (eq. (7))
ξ	transformed streamwise coordinate
$\tilde{\xi}$	similarity parameter
ρ	density
τ	total shear stress
Φ	shear parameter (eq. (23))
ϕ	circumferential angle

ω dummy variable

ω_s surface streamline angle

Subscripts:

e boundary-layer edge quantity

i,j,k grid point indices

p,q,r dummy indices

w wall value ($\zeta = 1$)

ξ,η direction of quantity

A bar over a symbol designates a dimensional quantity.

GOVERNING EQUATIONS

The governing equations are written in general form as follows (see fig. 1 for coordinate system; bar over a symbol designates a dimensional quantity):

Continuity

$$\frac{\partial}{\partial\xi}\left(\bar{h}_2\bar{h}_3\bar{\rho}\bar{u}\right) + \frac{\partial}{\partial\eta}\left(\bar{h}_1\bar{h}_3\bar{\rho}\bar{v}\right) + \frac{\partial}{\partial\zeta}\left(\bar{h}_1\bar{h}_2\bar{\rho}\bar{w}\right) = 0 \tag{1}$$

ξ-momentum

$$\frac{\bar{u}}{\bar{h}_1}\frac{\partial\bar{u}}{\partial\xi} + \frac{\bar{v}}{\bar{h}_2}\frac{\partial\bar{u}}{\partial\eta} + \frac{\bar{w}}{\bar{h}_3}\frac{\partial\bar{u}}{\partial\zeta} - \bar{u}\bar{v}\bar{\kappa}_2 + \bar{v}^2\bar{\kappa}_1 = -\frac{1}{\bar{\rho}\bar{h}_1}\frac{\partial\bar{p}}{\partial\xi} + \frac{1}{\bar{\rho}\bar{h}_3}\frac{\partial}{\partial\zeta}\left(\frac{\bar{\mu}_{eff}}{\bar{h}_3}\frac{\partial\bar{u}}{\partial\zeta}\right) \tag{2}$$

η-momentum

$$\frac{\bar{u}}{\bar{h}_1}\frac{\partial\bar{v}}{\partial\xi} + \frac{\bar{v}}{\bar{h}_2}\frac{\partial\bar{v}}{\partial\eta} + \frac{\bar{w}}{\bar{h}_3}\frac{\partial\bar{v}}{\partial\zeta} + \bar{u}^2\bar{\kappa}_2 - \bar{u}\bar{v}\bar{\kappa}_1 = -\frac{1}{\bar{\rho}\bar{h}_2}\frac{\partial\bar{p}}{\partial\eta} + \frac{1}{\bar{\rho}\bar{h}_3}\frac{\partial}{\partial\zeta}\left(\frac{\bar{\mu}_{eff}}{\bar{h}_3}\frac{\partial\bar{u}}{\partial\zeta}\right) \tag{3}$$

Energy

$$\frac{\bar{u}}{\bar{h}_1}\frac{\partial\bar{T}}{\partial\xi} + \frac{\bar{v}}{\bar{h}_2}\frac{\partial\bar{T}}{\partial\eta} + \frac{\bar{w}}{\bar{h}_3}\frac{\partial\bar{T}}{\partial\zeta} = \frac{1}{\bar{\rho}\bar{c}_p}\left\{\left(\frac{\bar{u}}{\bar{h}_1}\frac{\partial p}{\partial\xi} + \frac{\bar{v}}{\bar{h}_2}\frac{\partial\bar{p}}{\partial\eta}\right) + \frac{\bar{\mu}_{eff}}{\bar{h}_3^2}\left[\left(\frac{\partial\bar{u}}{\partial\zeta}\right)^2 + \left(\frac{\partial\bar{v}}{\partial\zeta}\right)^2\right] + \frac{1}{\bar{h}_3}\frac{\partial}{\partial\zeta}\left(\frac{\bar{k}_{eff}}{\bar{h}_3}\frac{\partial\bar{T}}{\partial\zeta}\right)\right\} \tag{4}$$

where h_1, h_2, and h_3 represent the metric coefficients for the incremental arc length $d\bar{s}$; that is

$$d\bar{s}^2 = (\bar{h}_1\, d\xi)^2 + (\bar{h}_2\, d\eta)^2 + (\bar{h}_3\, d\zeta)^2 \tag{5}$$

The parameters $\bar{\kappa}_1$ and $\bar{\kappa}_2$ are the geodesic curvatures of the curves ξ = Constant and η = Constant, respectively; namely

$$\left.\begin{aligned} \bar{\kappa}_1 &= -\frac{1}{\bar{h}_1\bar{h}_2}\frac{\partial \bar{h}_2}{\partial \xi} \\ \bar{\kappa}_2 &= -\frac{1}{\bar{h}_1\bar{h}_2}\frac{\partial \bar{h}_1}{\partial \eta} \end{aligned}\right\} \tag{6}$$

The governing system is completed with the perfect gas equation of state and Sutherland's molecular viscosity law.

Closure of equations (1) to (4) requires that the effective viscosity $\bar{\mu}_{eff}$ and thermal conductivity $\bar{k}_{eff}$ be expressed in terms of the dependent variables. These relations are formulated as follows:

$$\bar{\mu}_{eff} = \bar{\mu}\left(1 + \frac{\bar{\epsilon}}{\bar{\mu}}\Gamma\right) \tag{7}$$

and

$$\bar{k}_{eff} = \frac{\bar{c}_p\bar{\mu}}{N_{Pr}}\left(1 + \frac{\bar{\epsilon}}{\bar{\mu}}\frac{N_{Pr}}{N_{Pr,t}}\Gamma\right) \tag{8}$$

where $\bar{\mu}$, $\bar{\epsilon}$, N_{Pr}, and $N_{Pr,t}$ represent the molecular viscosity, eddy viscosity, Prandtl number, and static turbulent Prandtl number, respectively. The streamwise intermittency function Γ (ref. 17) models the transitional region of flow and is a function of ξ and η; $0 \leq \Gamma \leq 1$. In the present analysis the initiation and completion of the transitional flow process are empirically specified; however, correlation relations could be directly incorporated into the computer code. The eddy viscosity is assumed to be a scalar function independent of coordinate direction (refs. 8 and 18). The following simple scalar invariant turbulence models are considered:

Single-layer mixing length model:

$$\bar{\epsilon} = \bar{\rho}\bar{\ell}_1^2\left\{\frac{1}{\bar{h}_3^2}\left[\left(\frac{\partial \bar{u}}{\partial \zeta}\right)^2 + \left(\frac{\partial \bar{v}}{\partial \zeta}\right)^2\right]\right\}^{1/2}\tilde{\gamma} \tag{9}$$

where

$$\frac{\bar{\ell}_1}{\bar{x}_{3,e}} = k_2 \tanh\left(\frac{k_1}{k_2}\frac{\bar{x}_3}{\bar{x}_{3,e}}\right) D \tag{10}$$

$$D = 1 - \exp\left(-\frac{\bar{x}_3}{A}\right) \tag{11}$$

$$\bar{A} = k_3\left(\frac{\bar{\mu}}{\bar{\rho}}\right)_w\left(\frac{\bar{\tau}}{\bar{\rho}}\right)_w^{-1/2} \tag{12}$$

$$\tilde{\gamma} = \frac{1 - \operatorname{erf}\left(k_5 \dfrac{\bar{x}_3}{\bar{x}_{3,e}} - k_6\right)}{2} \tag{13}$$

$$\bar{\tau} = \left(\bar{\tau}_\xi{}^2 + \bar{\tau}_\eta{}^2\right)^{1/2} \tag{14}$$

Two-layer eddy viscosity model:

Inner law

$$\epsilon_{inner} = \bar{\rho}\bar{\ell}_2{}^2\left\{\frac{1}{\bar{h}_3{}^2}\left[\left(\frac{\partial\bar{u}}{\partial\bar{\zeta}}\right)^2 + \left(\frac{\partial\bar{v}}{\partial\bar{\zeta}}\right)^2\right]\right\}^{1/2}\tilde{\gamma} \qquad \left(0 \leq \bar{x}_3 \leq \bar{x}_{3,c}\right) \tag{15}$$

Outer law

$$\epsilon_{outer} = k_4\bar{\rho}\bar{U}_{e,t}\bar{\delta}^*\tilde{\gamma} \qquad \left(\bar{x}_{3,c} < \bar{x}_3 \leq \bar{x}_{3,e}\right) \tag{16}$$

where

$$\bar{\ell}_2 = k_1\bar{x}_3 D \tag{17}$$

$$\bar{U}_{e,t} = \left(\bar{u}_e{}^2 + \bar{v}_e{}^2\right)^{1/2} \tag{18}$$

$$\bar{\delta}^* = \int_0^{\bar{x}_{3,e}}\left[1 - \frac{\left(\bar{u}^2 + \bar{v}^2\right)^{1/2}}{\bar{U}_{e,t}}\right] d\bar{x}_3 \tag{19}$$

The point where the inner and outer laws are matched $\bar{x}_{3,c}$ is obtained from the continuity of eddy viscosity. For the results presented in this paper, k_1, k_2, k_3, k_4, k_5, k_6, and $N_{Pr,t}$ were assigned values of 0.435, 0.09, 26, 0.0168, 5, 0.78, and 0.95, respectively. These represent the classical values generally accepted for equilibrium two-

dimensional boundary-layer flows (see refs. 3 and 4); however, note that although the assigned values are sufficient over a broad range of flow and wall boundary conditions, modifications are required for certain classes of flow. (See refs. 4 and 10, for example.)

TRANSFORMATION

The use of physical coordinates introduces a number of problems for three-dimensional boundary-layer flows which can be circumvented by the introduction of a suitable transformation. If physical coordinates are used, three main problems are encountered as follows: (1) the numerical procedure and resultant solution are sensitive to the mesh-point distribution in the two surface spatial coordinates $(\Delta\bar{x}_1$ and $\Delta\bar{x}_2)$; (2) the growth of the boundary layer in the streamwise $(\bar{x}_1)$ and cross-flow $(\bar{x}_2)$ directions requires the addition of nodal points in the $\bar{x}_3$-direction as the solution progresses (these two factors result in excessive computer processing time and/or computer code logic); and (3) initial data planes cannot be generated where the initial boundary-layer thickness is zero (for example, at the tip of a sharp body). Consequently, in the present procedure a transformation is introduced which avoids these problems and, in addition, minimizes the computer processing time and storage requirements.

Equations (1) to (19) are first nondimensionalized (see ref. 11 for definition of non-dimensional variables), and a similarity-type transformation is introduced for the normal coordinate and velocity as follows:

$$\bar{h}_3 = \tilde{\xi}\,\frac{\rho_e}{\rho}\,\frac{\bar{L}}{\sqrt{R_{\infty,L}}}\,h_3 \tag{20}$$

$$\bar{w} = \frac{1}{\tilde{\xi}\sqrt{R_{\infty,L}}}\,\frac{\rho_e}{\rho}\,\bar{u}_\infty w \tag{21}$$

where $\bar{u}_\infty$ is the reference velocity and for a sharp cone $\tilde{\xi} = \sqrt{\xi}$. The metric coefficients h_2 and h_3 are arbitrary functions of the coordinates. In order to cast the equations into Crocco-type form, the following function is defined:

$$\zeta = (1 - F)^{1/2} \tag{22}$$

where $F = u/u_e$. The continuity and ξ-momentum equations are combined to form the shear equation, where the shear parameter Φ is defined by

$$\Phi = -\frac{1}{h_3}\,\frac{\mu}{T}\left(1 + \frac{\epsilon}{\mu}\,\Gamma\right) \tag{23}$$

Consequently, F is replaced by Φ as a new dependent variable, and $H = w/u_e$ is uncoupled from the system. The governing system of equations reduces to three coupled

nonlinear partial differential equations in θ, G, and Φ together with an explicit algebraic relationship for H. The system assumes the following form:

$$\frac{\partial^2 \omega}{\partial \zeta^2} + \alpha_1 \frac{\partial \omega}{\partial \zeta} + \alpha_2 \omega + \alpha_3 + \alpha_4 \frac{\partial \omega}{\partial \xi} + \alpha_5 \frac{\partial \omega}{\partial \eta} = 0 \tag{24}$$

where ω represents θ, G, and Φ, and α_1, α_2, α_3, α_4, and α_5 are nonlinear coefficients.

The boundary conditions on equation (24) are as follows:

when $\zeta = 0$

$$\theta = 1 \qquad G = 1 \qquad \Phi = 0 \tag{25a}$$

when $\zeta = 1$

$$\left.\begin{aligned} &\theta = \theta_w \quad \text{or} \quad \left(\frac{\partial \theta}{\partial \zeta}\right)_w = f(\xi,\eta) \\ &G = 0 \\ &\left(\frac{\partial \Phi}{\partial \zeta}\right)_w = -\left(a_1 H + a_2 \frac{\bar{e}\theta}{\Phi} + \Phi\right)_w \end{aligned}\right\} \tag{25b}$$

where a_1 and a_2 are functions of geometry and the inviscid edge conditions.

The primary advantage of the Crocco-type transformation is that the solution domain is bounded between the definite limits $0 \leq \zeta \leq 1$. The only disadvantage of the transformation is that velocity overshoot in F is not allowed; that is, F must increase monotonically from the specified wall value (slip at the surface can be specified) to unity at the edge boundary. Edge vorticity and streamline swallowing are not considered in this paper.

SOLUTION TECHNIQUE

Equation (24) is solved in an iterative mode with a marching implicit finite-difference technique suggested by Dwyer (ref. 19) and modified by Krause (ref. 20). The method is second-order accurate and unconditionally stable (conditional stability for reverse cross flow; see ref. 20). For turbulent flows a minimum of two mesh points in the ζ-plane must be located in the viscous sublayer; consequently, a variable mesh-point distribution is used. In the present study a geometric progression is assumed; that is, $\Delta\zeta_{k+1}/\Delta\zeta_k = C$ for $\kappa = 2, 3, \ldots, N - 1$ (ref. 3). Variable mesh-point distributions are also used in the ξ- and η-planes to minimize the computer processing time and storage requirements. A schematic of the difference molecule is presented in figure 2. Equation (24) is written at the point (i-1/2,j,k) and solved for the values of the dependent

variables θ, G, Φ, and H at the point (i,j,k). Consequently, the partial derivatives of equation (24) at the point (i-1/2,j,k) are expressed as follows:

$$\left(\frac{\partial^2\omega}{\partial\zeta^2}\right)_{i-1/2,j,k} = \frac{\left(\frac{\partial^2\omega}{\partial\zeta^2}\right)_{i-1,j,k} + \left(\frac{\partial^2\omega}{\partial\zeta^2}\right)_{i,j,k}}{2} \tag{26}$$

$$\left(\frac{\partial\omega}{\partial\zeta}\right)_{i-1/2,j,k} = \frac{\left(\frac{\partial\omega}{\partial\zeta}\right)_{i-1,j,k} + \left(\frac{\partial\omega}{\partial\zeta}\right)_{i,j,k}}{2} \tag{27}$$

$$\left(\frac{\partial\omega}{\partial\xi}\right)_{i-1/2,j,k} = \frac{\omega_{i,j,k} - \omega_{i-1,j,k}}{\Delta\xi_{i-1}} \tag{28}$$

$$\left(\frac{\partial\omega}{\partial\eta}\right)_{i-1/2,j,k} = \frac{\frac{\omega_{i-1,j+1,k} - \omega_{i-1,j,k}}{\Delta\eta_j} + \frac{\omega_{i,j,k} - \omega_{i,j-1,k}}{\Delta\eta_{j-1}}}{2} \tag{29}$$

$$(\omega)_{i-1/2,j,k} = \frac{\omega_{i-1,j,k} + \omega_{i,j,k}}{2} \tag{30}$$

The derivative quantities in equations (26) and (27) are obtained from

$$\left(\frac{\partial^2\omega}{\partial\zeta^2}\right)_{p,q,r} = Y_1\omega_{p,q,r+1} - Y_2\omega_{p,q,r} + Y_3\omega_{p,q,r-1} \tag{31}$$

$$\left(\frac{\partial\omega}{\partial\zeta}\right)_{p,q,r} = Y_4\omega_{p,q,r+1} - Y_5\omega_{p,q,r} - Y_6\omega_{p,q,r-1} \tag{32}$$

where

$$Y_1 = \frac{2}{\Delta\zeta_r(\Delta\zeta_r + \Delta\zeta_{r-1})} \tag{33}$$

$$Y_2 = \frac{2}{\Delta\zeta_r\,\Delta\zeta_{r-1}} \tag{34}$$

$$Y_3 = \frac{2}{\Delta\zeta_{r-1}(\Delta\zeta_r + \Delta\zeta_{r-1})} \tag{35}$$

$$Y_4 = \frac{\Delta\zeta_{r-1}}{\Delta\zeta_r(\Delta\zeta_r + \Delta\zeta_{r-1})} \tag{36}$$

$$Y_5 = \frac{\Delta\zeta_{r-1} - \Delta\zeta_r}{\Delta\zeta_r \, \Delta\zeta_{r-1}} \tag{37}$$

$$Y_6 = \frac{\Delta\zeta_r}{\Delta\zeta_{r-1}(\Delta\zeta_r + \Delta\zeta_{r-1})} \tag{38}$$

For equally spaced mesh-point distributions in the ζ-plane, equations (33) to (38) assume the values

$$\left.\begin{aligned} Y_1 &= \frac{1}{\Delta\zeta^2} & Y_2 &= 2Y_1 \\ Y_3 &= Y_1 & Y_4 &= \frac{1}{2\Delta\zeta} \\ Y_5 &= 0 & Y_6 &= Y_4 \end{aligned}\right\} \tag{39}$$

When a converged solution cannot be obtained at the most leeward plane, $\phi = 180^o$ (for example, for separation on leeward surface), a cubic Crank-Nicolson differencing scheme is used at the maximum η-station (ref. 14). If this procedure were not incorporated into the program logic, one η-station would be lost for each incremental $\Delta\xi$ because of the Krause differencing scheme; that is, equation (29) assumes the existence of a converged solution at the point (i-1,j+1,k) for $K = 2, 3, \ldots, N - 1$.

The marching procedure cannot be initiated without the existence of two orthogonal initial data planes. For a sharp right circular cone these planes of initial data are generated directly from the governing equations by using a second-order Crank-Nicolson scheme for the two planes $\xi = 0$, $0 \leq \eta \leq \eta_{max}$ and $0 \leq \xi \leq \xi_{max}$, $\eta = 0$ where similarity exists. A discussion of problems associated with obtaining initial data planes for general configurations is presented in reference 10.

Substitution of equations (26) to (30) into equation (24) results in a system of coupled algebraic equations whose coefficient matrix is of tridiagonal form which can be efficiently solved for the dependent variables (Thomas' algorithm). The primary problem associated with equation (24) is that the coefficients (α_1, α_2, etc.) are highly nonlinear. The shear equation controls the convergence rate of the numerical procedure (iterations required) as the system is sequentially iterated. Equation (24) can be written for Φ as

$$\frac{\partial^2\Phi}{\partial\zeta^2} + \left(\frac{h_1}{\zeta} + \frac{\beta_1}{\Phi^2}\right)\frac{\partial\Phi}{\partial\zeta} - \frac{h_1}{\zeta^2}\Phi + \frac{\beta_2}{\Phi} + \frac{\beta_3}{\Phi^2}\frac{\partial\Phi}{\partial\zeta} + \frac{\beta_4}{\Phi^2}\frac{\partial\Phi}{\partial\eta} = 0 \tag{40}$$

where β_1, β_2, β_3, and β_4 are functions of geometry, inviscid edge conditions, and previous iterate values of the dependent variables F and θ and their derivatives. The problem is further complicated by the inclusion of the turbulence models (eqs. (9) to (19)), since in the transformed plane Φ appears explicitly in the transformed relationships.

Consequently, the coefficients (β_1, β_2, etc.) also depend on Φ for turbulent flows (for laminar flows this dependence is removed). The system of equations will not converge if the shear equation is written as shown in equation (40) because of the Φ^{-1} term. Convergence can be achieved by using a Taylor's series expansion of Φ^{-1} about the previous iterate value Φ_G; that is

$$\frac{1}{\Phi} = \frac{1}{\Phi_G}\left(2 - \frac{\Phi}{\Phi_G}\right) + O(\Phi^2) \tag{41}$$

Substitution of equation (41) into equation (40) yields

$$\frac{\partial^2 \Phi}{\partial \zeta^2} + \left(\frac{h_1}{\zeta} + \frac{\beta_1}{\Phi^2}\right)\frac{\partial \Phi}{\partial \zeta} + \left(-\frac{h_1}{\zeta^2} - \frac{\beta_2}{\Phi_G{}^2}\right)\Phi + 2\,\frac{\beta_2}{\Phi_G} + \frac{\beta_3}{\Phi^2}\frac{\partial \Phi}{\partial \zeta} + \frac{\beta_4}{\Phi^2}\frac{\partial \Phi}{\partial \eta} = 0 \tag{42}$$

Equation (42) converges in an average of five to seven iterations for high Reynolds number turbulent flow. The wall boundary condition on Φ (see eq. (25b)) also presents a problem since Φ_w is unknown; however, the wall derivative relationship can be directly incorporated in the iterative solution procedure. In principle, it should be possible to reduce the average number of iterations substantially to a maximum of three. Research continues in the areas of (1) restructuring equation (42), (2) treatment of the Φ wall boundary conditions, and (3) the problem associated with Φ in the transformed turbulence models. Note however that the present procedure requires essentially the same processing time per mesh point (0.002 sec) as the Cebeci-Keller Box method (ref. 10) and that this time may be substantially reduced through convergence accelerator procedures and/or the inclusion of Newton-Raphson iteration.

RESULTS AND DISCUSSION

The numerical procedure and turbulence models have been applied to a number of flows (current geometry limited to sharp right circular and elliptic cones). In this paper, numerical results are compared with experimental wall and profile data for a cone with a 12.5° semiapex angle at an angle of attack of 15.75°. The free-stream Mach number, total pressure, and total temperature were 1.8, 172.4 kN/m^2, and 294 K, respectively. Transition was assumed to be initiated and completed in the region $0.03 \leq \bar{x}_1/\bar{L} \leq 0.08$ ($\bar{L}$ = 105.6 cm). The adiabatic wall boundary condition was imposed on the energy equation (see eq. (25b)); that is, $\left(\frac{\partial \theta}{\partial \zeta}\right)_w = 0$. No experimental data were input into the viscous flow solution. The inviscid pressure distribution $p_e = p_e(\xi,\eta)$ was obtained from a numerical solution of the three-dimensional inviscid flow equations. Experimental data for verification of the accuracy of the numerical procedure and turbulence models were obtained from reference 21.

The numerical results for F, G, and θ are compared with experimental data in figure 3 for circumferential locations of $\phi = 0^o$, 45^o, 90^o, and 135^o. In order to evaluate the effect of nodal-point spacing in the ζ-plane, a parametric study was made for N = 301, 201, 101, 61, and 21 with $\Delta\zeta_{k+1}/\Delta\zeta_k = 1.02$. The results for N = 301 and 201 were essentially identical, and those for N = 101 were within 0.5 percent of the N = 301 results. The agreement between the experimental and numerical results is very good for 301 points and, in general, good for 21 points. The two turbulence models (eqs. (9) to (19)) produced essentially identical results. The two-layer model results presented in figure 3 are for N = 301; however, the two-layer results for N = 21 were essentially identical to the N = 21 results of the single-layer model. A comparison of the numerical results for $C_{f,e}$ presented in figure 4(a) indicates that the difference between the results for 61 points and 301 points is approximately 1 percent and between 21 points and 301 points is approximately 3 percent. In figure 4(b), $C_{f,e}$ is presented as a function of ϕ. Figures 3 and 4 indicate that as few as 21 points normal to the wall boundary can be used to obtain results to within 3-percent accuracy (compared with N = 301 results). Numerical results for surface streamline direction $\omega_s = \tan^{-1}\left(\tau_\eta/\tau_\xi\right)_w$ obtained for N = 301 and 21 are compared with experimental data in figure 5. The agreement is good considering that the inviscid pressure distribution was obtained from the inviscid equations and not from experimental data; that is, displacement surface effects are not included in the viscous/inviscid calculations.

The major points which should be noted in these comparisons are (1) that the numerical procedure is efficient and accurate and (2) that the turbulence models are satisfactory for high Reynolds number equilibrium turbulent boundary-layer flows. The Crocco-type transformation and the numerical procedure allow the generation of accurate solutions for a minimum of 21 points normal to the wall boundary. The computer code requires 60000_8 storage (the i-1,j,k data plane is stored on disk) and approximately 0.002 second per grid point processing time on a CDC 6600 computer system. Current studies indicate that it may be possible to substantially reduce the processing time through convergence accelerators for the shear equation (eq. (42)) and/or the inclusion of a Newton-Raphson iteration procedure. The current program is comparable in both storage and processing time with the Cebeci-Keller Box method (ref. 10).

CONCLUDING REMARKS

Solutions of the compressible three-dimensional turbulent boundary-layer equations have been obtained and compared with experimental data. The agreement between the numerical results and experimental data indicates that accurate results can be obtained with a minimum of 21 nodal points in the plane normal to the wall boundary layer for high Reynolds number equilibrium turbulent flows. The turbulence models, although simple in

concept, were adequate for the class of flow considered; however, previous experience indicates that caution should be exercised in extending these models to more demanding boundary-layer flows. The numerical procedure is second-order accurate and unconditionally stable (conditional stability for reverse cross flow). The computer code requires 60000_8 storage and approximately 0.002 second per grid point processing time (CDC 6600 computer system). Studies indicate that the processing time may be further reduced through convergence accelerator and Newton-Raphson iteration procedures; however, the current computer requirements of storage and speed compare favorably with other procedures under development.

REFERENCES

1. Kline, S. J.; Morkovin, M. V.; Sovran, G.; and Cockrell, D. J., eds.: Computation of Turbulent Boundary Layers – 1968 AFOSR-IFP-Stanford Conference. Vol. I – Methods, Predictions, Evaluation and Flow Structure. Stanford Univ., c.1969.

2. Compressible Turbulent Boundary Layers. NASA SP-216, 1969.

3. Harris, Julius E.: Numerical Solution of the Equations for Compressible Laminar, Transitional, and Turbulent Boundary Layers and Comparisons With Experimental Data. NASA TR R-368, 1971.

4. Cebeci, Tuncer; and Smith, A. M. O.: Analysis of Turbulent Boundary Layers. Academic Press, Inc., 1974.

5. Raetz, G. S.: A Method of Calculating Three-Dimensional Laminar Boundary Layers of Steady Compressible Flows. Rep. No. NAI-58-73, Northrop Aircraft, Inc., Dec. 1957.

6. Wang, K. C.: On the Determination of the Zones of Influence and Dependence for Three-Dimensional Boundary-Layer Equations. J. Fluid Mech., vol. 48, no. 2, July 28, 1971, pp. 397-404.

7. Bradshaw, P.: Effects of Streamline Curvature on Turbulent Flow. AGARDograph No. 169, Aug. 1973.

8. Nash, John F.; and Patel, Virendra C.: Three-Dimensional Turbulent Boundary Layers. Sci. & Business Consultants, Inc., 1972.

9. Bradshaw, P. (appendix by V. C. Patel): The Strategy of Calculation Methods for Complex Turbulent Flows. Rep. No. 73-05, Aeronaut. Dep., Imp. Coll. Sci. & Technol., Aug. 1973.

10. Cebeci, Tuncer; Kaups, Kalle; Mosinskis, G. J.; and Rehn, J. A.: Some Problems of the Calculation of Three-Dimensional Boundary-Layer Flows on General Configurations. NASA CR-2285, 1973.

11. McGowan, J. J., III; and Davis, R. T.: Development of a Numerical Method To Solve the Three-Dimensional Compressible Laminar Boundary-Layer Equations With Application to Elliptical Cones at Angle of Attack. ARL 70-0341, U.S. Air Force, Dec. 1970.

12. Adams, John C., Jr.: Analysis of the Three-Dimensional Compressible Turbulent Boundary Layer on a Sharp Cone at Incidence in Supersonic and Hypersonic Flow. AEDC-TR-72-66, U.S. Air Force, June 1972. (Available from DDC as AD 743 003.)

13. Popinski, Zenon; and Davis, R. T.: Three-Dimensional Compressible Laminar Boundary Layers on Sharp and Blunt Circular Cones at Angle of Attack. NASA CR-112316, 1973.

14. Blottner, F. G.; and Ellis, Molly: Three-Dimensional, Incompressible Boundary Layer on Blunt Bodies. Part I: Analysis and Results. SLA-73-0366, Sandia Corp., Apr. 1973.

15. Wang, K. C.: Three-Dimensional Laminar Boundary Layer Over Body of Revolution at Incidence. Part VI. General Methods and Results of the Case of High Incidence. AFOSR-TR-73-1045, U.S. Air Force, May 1973. (Available from DDC as AD 763 831.)

16. Blottner, F. G.: Computational Techniques for Boundary Layers. Paper for AGARD Lecture Series 73 on Computational Methods for Inviscid and Viscous Two- and Three-Dimensional Flow Fields (Von Karman Inst.), Feb. 17-22, 1975.

17. Dhawan, S.; and Narasimha, R.: Some Properties of Boundary Layer Flow During the Transition From Laminar to Turbulent Motion. J. Fluid Mech., vol. 3, pt. 4, Jan. 1958, pp. 418-436.

18. Hunt, James L.; Bushnell, Dennis M.; and Beckwith, Ivan E.: The Compressible Turbulent Boundary Layer on a Blunt Swept Slab With and Without Leading-Edge Blowing. NASA TN D-6203, 1971.

19. Dwyer, Harry A.: Solution of a Three-Dimensional Boundary-Layer Flow With Separation. AIAA J., vol. 6, no. 7, July 1968, pp. 1336-1342.

20. Krause, Egon: Comment on "Solution of a Three-Dimensional Boundary-Layer Flow With Separation." AIAA J., vol. 7, no. 3, Mar. 1969, pp. 575-576.

21. Rainbird, William John: Turbulent Boundary-Layer Growth and Separation on a Yawed Cone. AIAA J., vol. 6, no. 12, Dec. 1968, pp. 2410-2416.

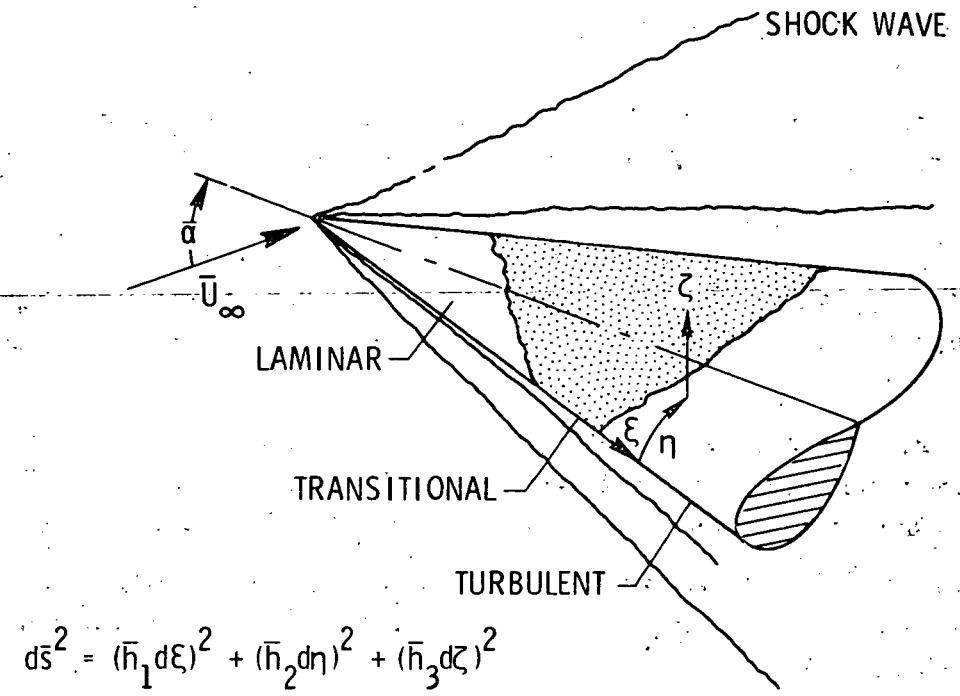

Figure 1.- Coordinate system.

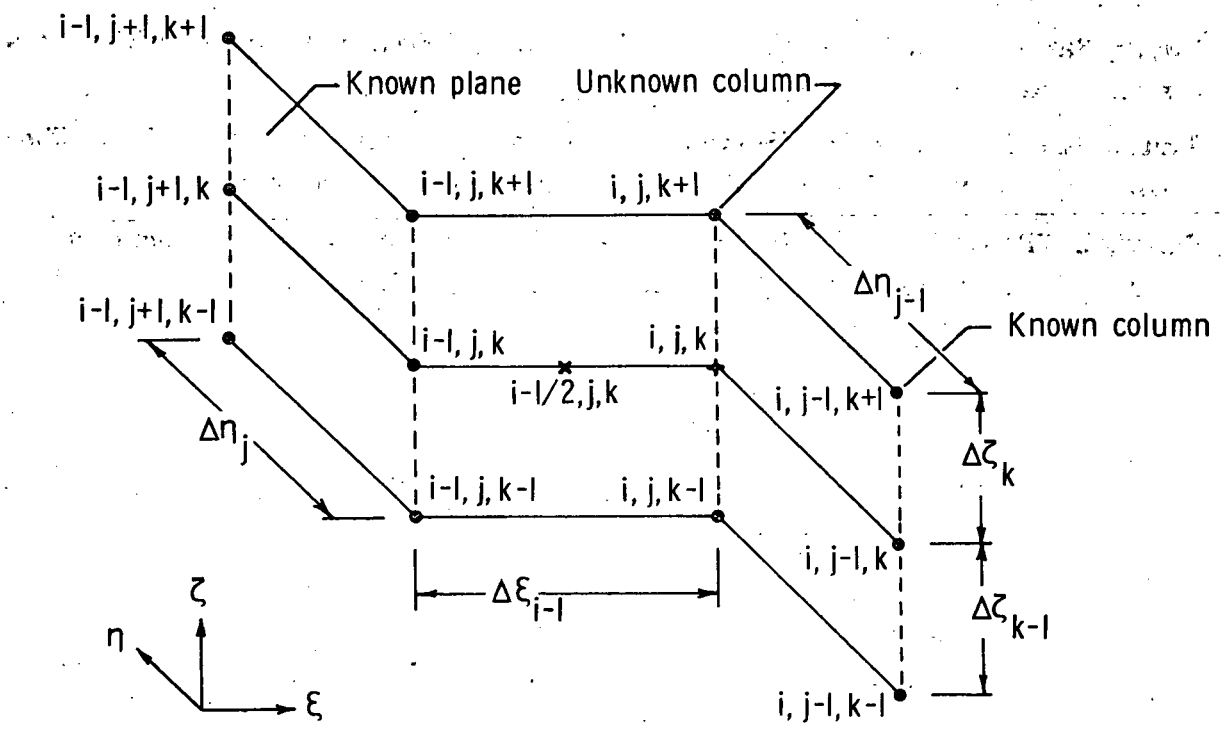

Figure 2.- Difference grid nomenclature.

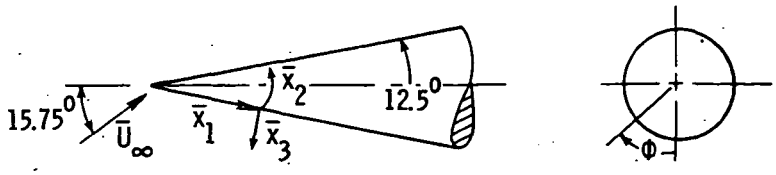

Experimental data		Numerical results	N
○	u/Q_e	Mixing length model	
□	v/Q_e	———	301
△	T/T_e	- - - - - - - - - -	21
		Eddy viscosity model	
		x	301

STORAGE/PROCESSING ON CDC 6600 COMPUTER

N	CPU time per mesh point, sec	Storage	Total CPU time, sec
301	0.002	170000_8	900
21	.002	60000_8	60

(a) Details of figure 3.

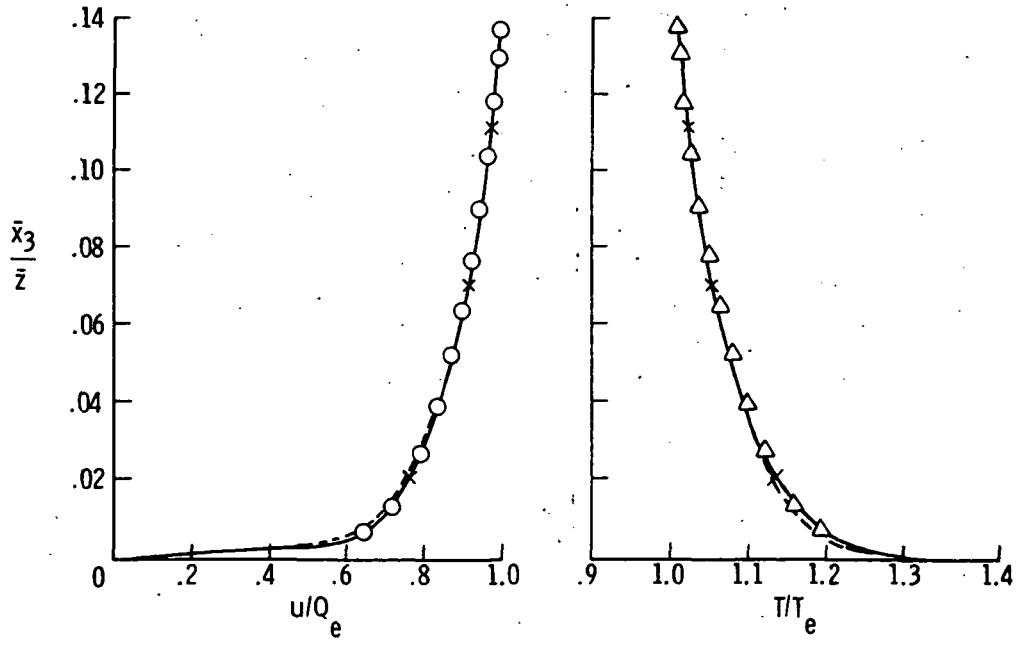

(b) $\phi = 0°$.

Figure 3.- Profile comparisons. $M_\infty = 1.8$; $R_{\infty,\bar{L}} = 25 \times 10^6$; $\gamma = 1.4$; $\bar{z} = 2.54$ cm; $\bar{L} = 105.6$ cm; $Q_e = \sqrt{u_e^2 + v_e^2}$.

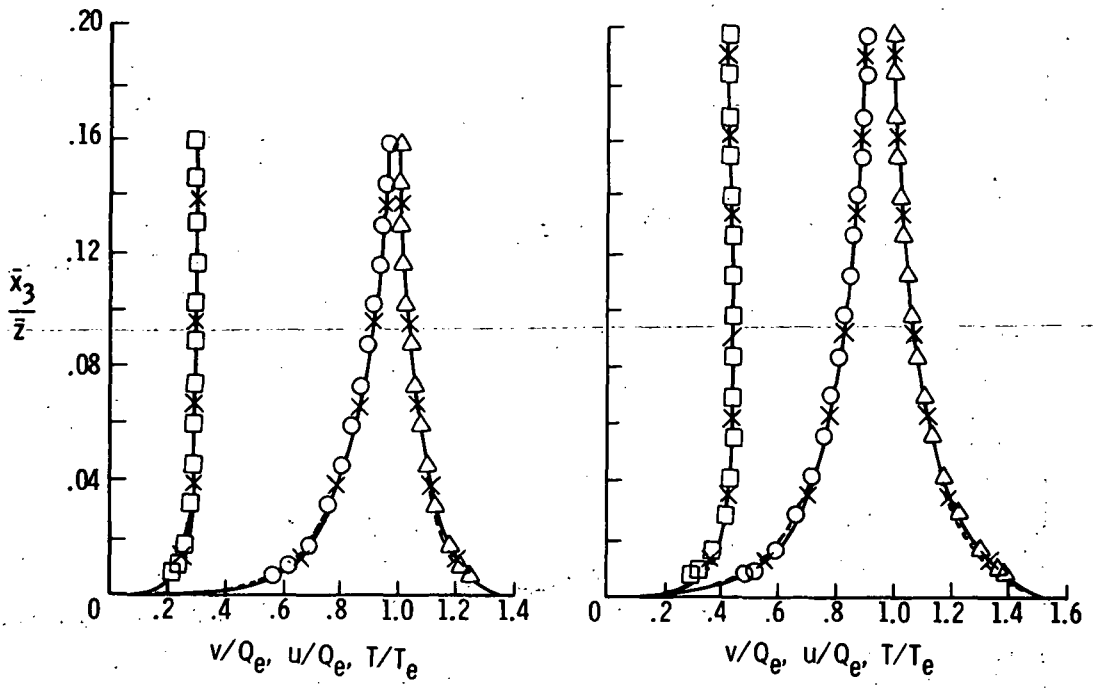

(c) $\phi = 45^o$.

(d) $\phi = 90^o$.

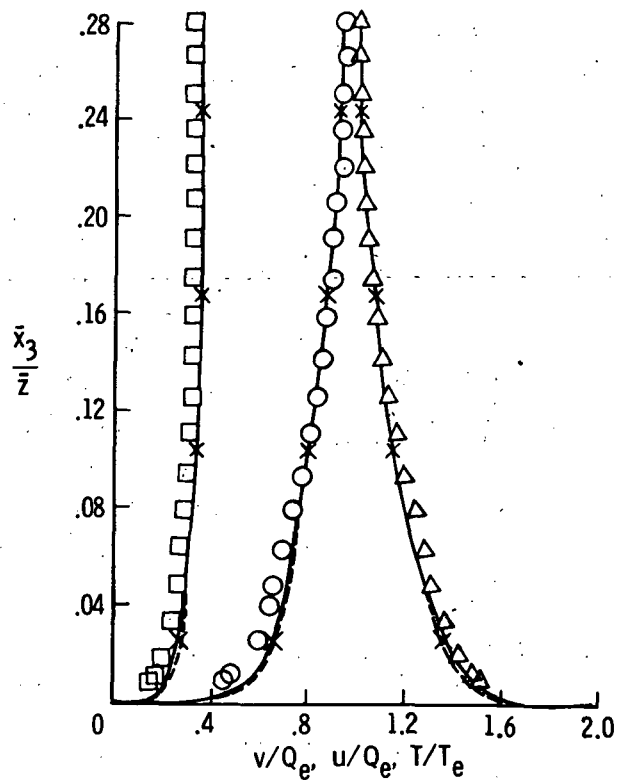

(e) $\phi = 135^o$.

Figure 3.- Concluded.

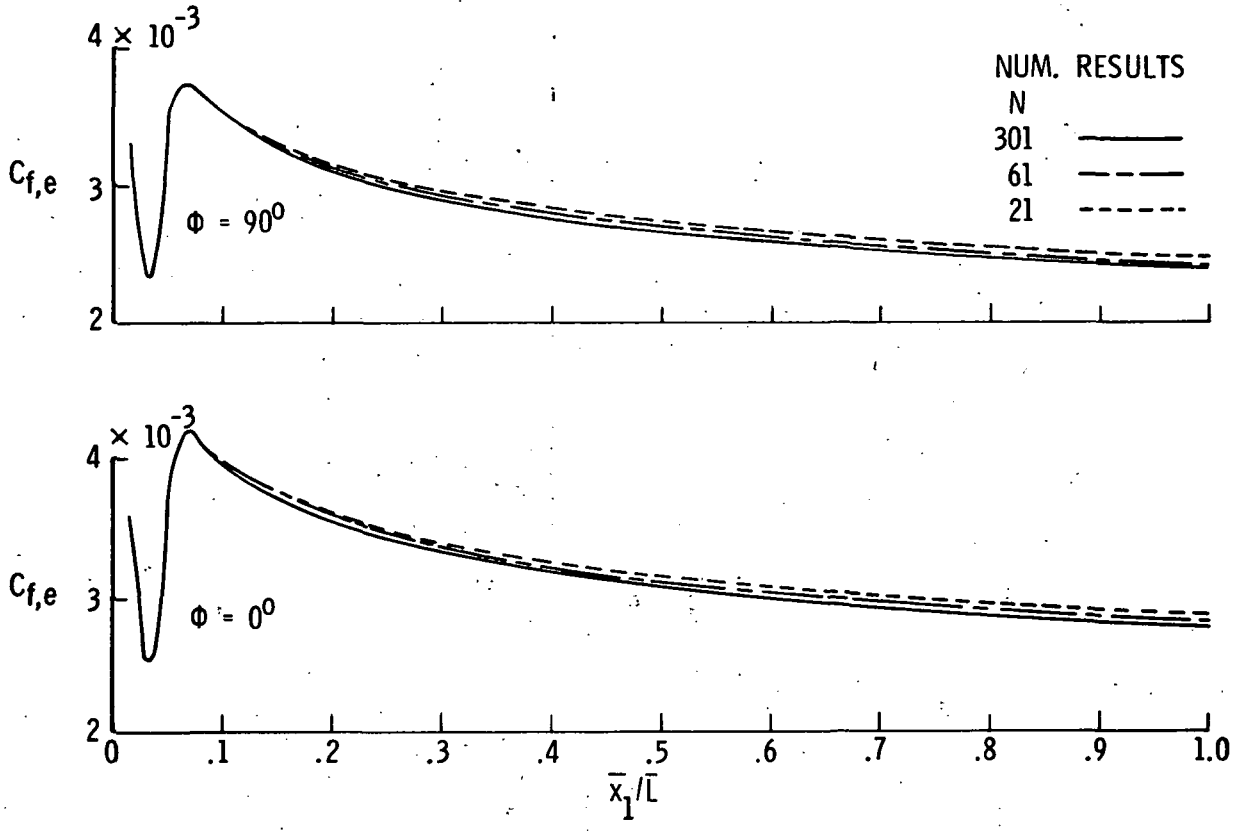

(a) $\phi = 0^{o}; 90^{o}$.

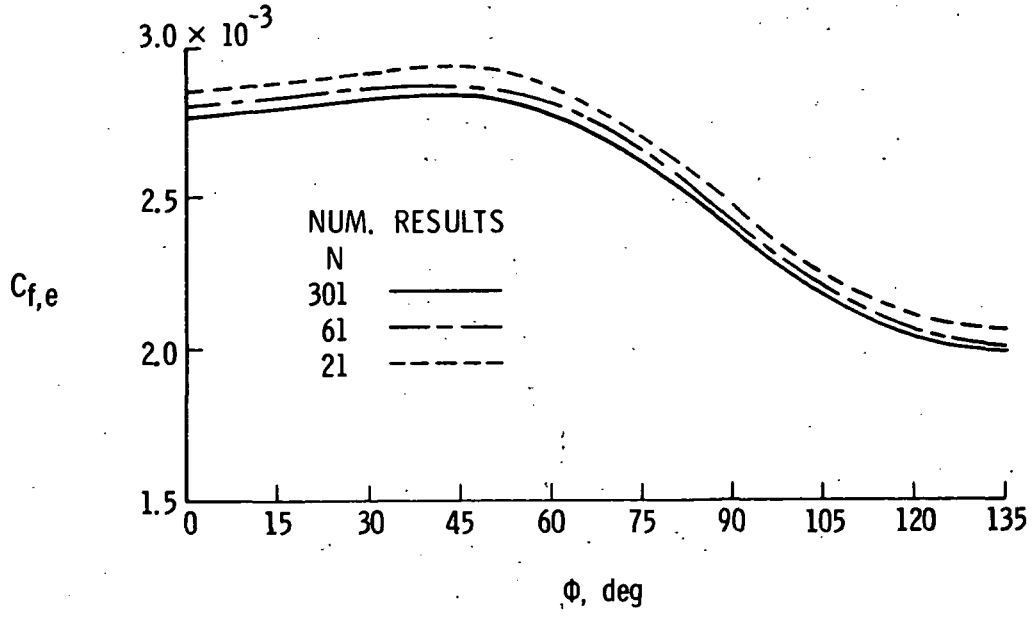

(b) $\bar{x}_1/\bar{L} = 1$.

Figure 4.- Effect of nodal spacing on skin friction.

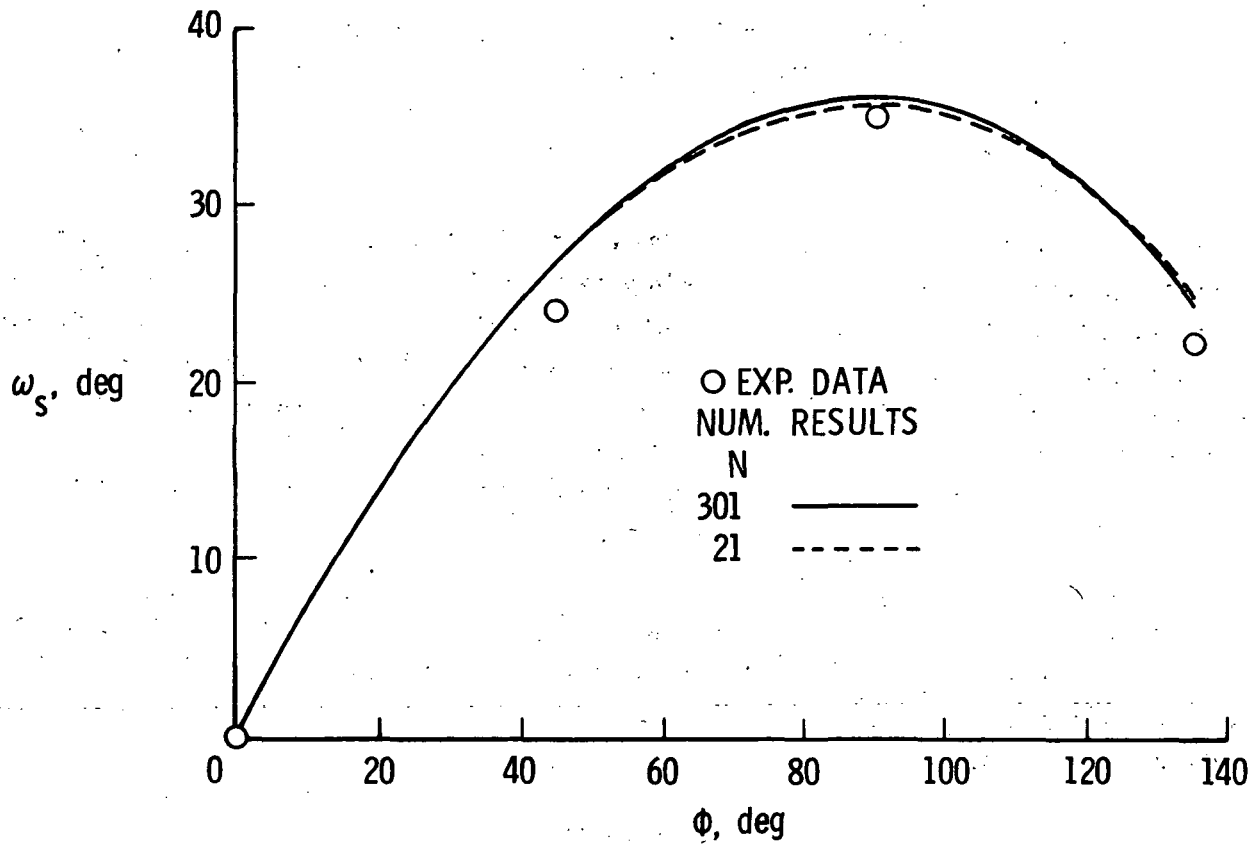

Figure 5.- Surface flow direction. $\bar{x}_1/\bar{L} = 1$.